Action of DNA Repair Endonuclease ERCC1/XPF in Living Cells

Adriaan B. Houtsmuller,[1]* Suzanne Rademakers,[2] Alex L. Nigg,[1] Deborah Hoogstraten,[2] Jan H. J. Hoeijmakers,[2]† Wim Vermeulen[2]*

To study the nuclear organization and dynamics of nucleotide excision repair (NER), the endonuclease ERCC1/XPF (for excision repair cross complementation group 1/xeroderma pigmentosum group F) was tagged with green fluorescent protein and its mobility was monitored in living Chinese hamster ovary cells. In the absence of DNA damage, the complex moved freely through the nucleus, with a diffusion coefficient (15 ± 5 square micrometers per second) consistent with its molecular size. Ultraviolet light–induced DNA damage caused a transient dose-dependent immobilization of ERCC1/XPF, likely due to engagement of the complex in a single repair event. After 4 minutes, the complex regained mobility. These results suggest (i) that NER operates by assembly of individual NER factors at sites of DNA damage rather than by preassembly of holocomplexes and (ii) that ERCC1/XPF participates in repair of DNA damage in a distributive fashion rather than by processive scanning of large genome segments.

Nucleotide excision repair (NER) is a sophisticated DNA repair mechanism that eliminates a wide range of structurally unrelated DNA lesions (*1*). The most common types of DNA damage targeted by NER are cyclobutane pyrimidine dimers and (6-4) photoproducts (6-4PPs), both produced by the ultraviolet (UV) component of sunlight (*1*). The major NER pathway operates across the genome (global genome NER), whereas transcription-coupled NER preferentially repairs lesions that block transcription (*2*). Genetic defects in NER are associated with three diseases characterized by photosensitivity: xeroderma pigmentosum (XP), Cockayne syndrome, and trichothiodystrophy (*3*). Global genome NER is initiated by the DNA-damage–binding factor XPC/hHR23B (*4*), and transcription-coupled NER by RNA polymerase stalled at a lesion (*2*). TFIIH, XPA, and RPA (*5, 6*) are then recruited, resulting in local opening of the DNA helix, proper orientation of the NER machinery, and stabilization of the opened DNA intermediate. The single-strand–binding protein (RPA), bound to the nondamaged DNA strand, helps to position (*6*) the structure-specific endonucleases XPG (which makes the 3′ incision) (*7*) and the ERCC1/XPF complex (which makes the 5′ incision) (*8*). After excision of the damage, the resulting gap is filled in by DNA polymerase δ/ε and auxiliary factors (*1, 9*).

It is not known whether NER operates in intact cells as a preassembled holocomplex (*10*), or by consecutive assembly of subcomplexes (*11*) or individual NER factors at sites of DNA damage. It is also unclear whether NER proteins find DNA damage by processive scanning of large genome segments or in a distributive fashion by diffusion. To address these questions, we fused the green fluorescent protein (GFP) (*12*) to the ERCC1 subunit of the 5′ endonuclease ERCC1/XPF (*13*) so that we could study repair in living cells. The fusion gene (*ERCC1-GFP*) was stably transfected into ERCC1-deficient Chinese hamster ovary (CHO) cells (43-3B) (Fig. 1D). Immunoblot and immunoprecipitation analyses showed that ERCC1 was detectable only in the GFP-tagged form (Fig. 1A) and was expressed at the same level as endogenous ERCC1 in repair-competent HeLa cells and 43-3B cells corrected by natural *ERCC1* (Fig. 1A). The ERCC1-GFP associated with XPF (Fig. 1B); formation of this complex has been shown to be required for the stabilization of both proteins (*8, 14*). Transfection of ERCC1-GFP fully corrected the extreme UV sensitivity (and other repair defects) (*15*) of 43-3B cells (Fig. 1C). These data demonstrate that the fusion protein was expressed at physiological levels, was complexed with XPF, and its function was not affected by the GFP tag.

Confocal microscopy of living 43-3B cells revealed a predominantly homogeneous nuclear distribution of ERCC1-GFP/XPF, although 26 ± 7% of the nuclei contained one to three bright fluorescent spots (Fig. 1E). After induction of DNA repair following UV exposure (8 J/m^2), we did not detect any significant alterations in the homogeneous fluorescence pattern, whereas the number of nuclei containing spots decreased to 9 ± 2%. These observations contrast with previous work using immunofluorescence or repair-patch labeling, which showed nonrandom distribution of NER proteins or sites of repair in the nucleus (*16, 17*). The function of the bright fluorescent spots is unclear. They were not artifacts of GFP tagging or ERCC1-GFP overexpression, because they were also detected by antibodies to ERCC1 in 30 to 40% of HeLa cells expressing endogenous ERCC1 (Fig. 1F). Since the spots are present in a fraction of the cells, a general role in enzyme storage is not likely.

To determine whether ERCC1 is mobile or fixed, we studied the nuclear mobility of ERCC1-GFP/XPF using FRAP (fluorescence redistribution after photobleaching) technology (*18, 19*). The diffusion coefficient (*D*) was determined by measuring the movement of fluorescent ERCC1-GFP/XPF into a previously bleached strip through the nucleus, as described (*19*). The method was first calibrated with cells expressing enhanced GFP (EGFP) (*13*), and the measured *D* value (58 ± 9 μm^2/s) was in the range of a previously reported value (*19*).

In the absence of DNA damage, ERCC1-GFP/XPF moved freely through the nucleus of CHO cells. The measured diffusion coefficient (15 ± 5 μm^2/s) was consistent with the size of ERCC1-GFP/XPF (163 kD) (*20*), suggesting that the majority of ERCC1/XPF is not part of a large NER holocomplex. Free mobility was also found for other NER proteins tagged with EGFP: XPA-EGFP (70 kD, D = 28 ± 5 μm^2/s) and XPB-EGFP (>400 kD in TFIIH, D = 6.2 ± 4 μm^2/s) (*21*); the observed *D*'s were in agreement with the known size of the respective NER protein (complexes) (Fig. 1G) (*20, 21*). These findings argue against a model in which NER proteins are fixed to nuclear structures in the absence of damage.

To study the effect of DNA damage on ERCC1-GFP/XPF mobility, we developed a technology based on FRAP (*19*) (designated FRAP-FIM) (Fig. 2). Briefly, the fluorescence ratio of confocal sections before and 4 s after spot bleaching (which takes 4 s) was plotted as a function of the distance to the bleached spot [fluorescence ratio profile (FRP)], (Fig. 2D). The method was validated with fixed and living SV40 (simian virus 40)–transformed human fibroblasts expressing EGFP. Fixed human fibroblasts expressing EGFP showed no bleaching outside the laser beam area (Fig. 3, A and B), and the experimentally obtained FRP (Fig. 3C) matched the theoretically predicted curve (Fig. 2D). In contrast, in living hu-

[1]Department of Pathology (Josephine Nefkens Institute) and [2]Department of Cell Biology and Genetics (Medical Genetics Center, CBG), Erasmus University, Post Office Box 1738, 3000 DR Rotterdam, Netherlands.

*These authors contributed equally to this work.
†To whom correspondence should be addressed. E-mail: Hoeijmakers@gen.fgg.eur.nl

man fibroblasts, an average of 60% of the EGFP molecules in the nucleus passed through the laser cone volume during 4 s of spot bleaching and lost fluorescence. The remaining fluorescence was uniformly redistributed within the nucleus 4 s after spot bleaching, resulting in the predicted horizontal FRP (Fig. 3, D to F). Control experiments indicated that the FRAP-FIM procedure did not affect cell viability (*15*).

We then applied FRAP-FIM to the ERCC1-GFP–expressing CHO cells. The FRPs of fixed and living cells (Fig. 3, G to L) showed curves similar to those of fibroblasts expressing free EGFP (Fig. 3, C and F). To

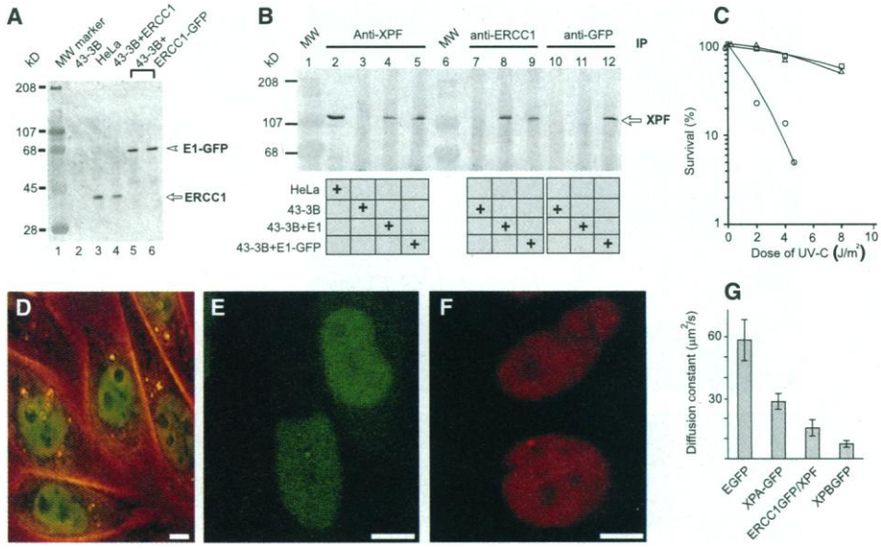

Fig. 1. Expression and functionality of ERCC1-GFP (*13*) in CHO 43-3B cells. Cell lines used: HeLa (repair-proficient), 43-3B (ERCC1-deficient, UV-sensitive), 43-3B + ERCC1 (43-3B stably expressing nontagged ERCC1, repair-proficient), and 43-3B + ERCC1-GFP (43-3B stably expressing ERCC1-GFP). (**A**) Immunoblot of whole-cell extracts (WCE) (*28*) of transfected and control cell lines (10 μg of protein per lane), probed with polyclonal anti-ERCC1. Arrow, untagged ERCC1; arrowhead, ERCC1-GFP. (**B**) Immunoblot, probed with anti-XPF (polyclonal), showing immunoprecipitations (IP) of WCE from the indicated cell lines. Immunocomplexes were bound to protein A–sepharose beads and separated by SDS–polyacrylamide gel electrophoresis. IPs were performed with anti-XPF (lanes 2 to 5), anti-ERCC1 (lanes 7 to 9), and anti-GFP (lanes 10 to 12). Lanes 1 and 6 contained markers for molecular size (MW, indicated at left in kilodaltons). (**C**) Survival of 43-3B cells (circles), 43-3B + ERCC1-GFP cells (squares), and repair-proficient CHO-9 cells (triangles) after treatment with UV irradiation. (**D**) Combined phase-contrast (red) and fluorescence (green) image of ERCC1-GFP–transfected 43-3B cells. (**E**) Confocal image of ERCC1-GFP–transfected 43-3B cells, showing a homogeneous distribution of ERCC1. The lower nucleus shows a bright fluorescent spot (see text). (**F**) Confocal image of HeLa cells treated with polyclonal anti-ERCC1 antiserum (and stained with Cy-3–labeled secondary antibody), showing ERCC1 distribution and spots similar to the GFP fluorescence displayed in (E). (**G**) Diffusion constants of EGFP (27 kD) and three NER proteins, XPA-GFP (70 kD), ERCC1-GFP/XPF (163 kD), and XPB-GFP (>400 kD in TFIIH), showing a decrease of mobility with increasing molecular weight. Bars in (D), (E), and (F): 5 μm.

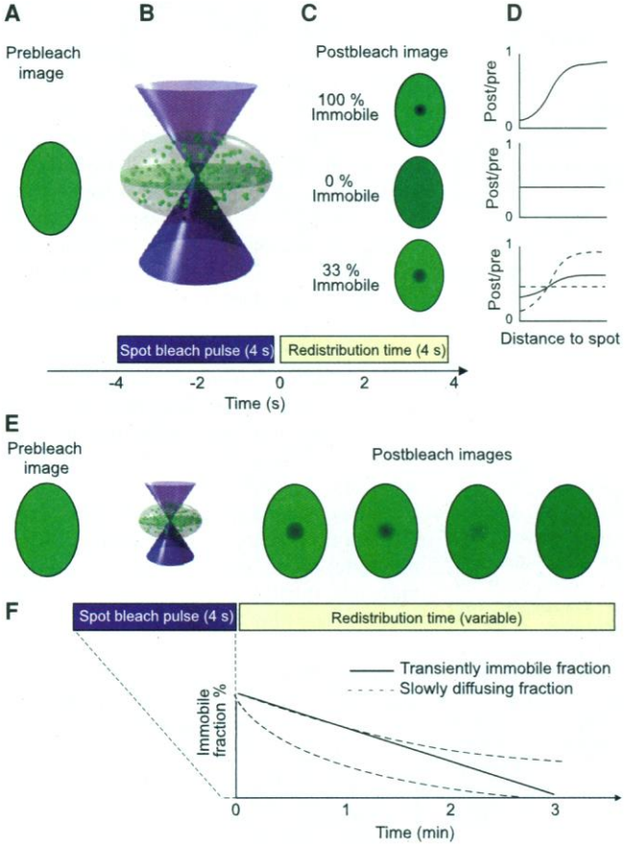

Fig. 2. FRAP-FIM protocols for quantitation of immobilized molecules in living cells. (A to D) Procedure for measurement of the immobile fraction. (**A**) Theoretical prebleach fluorescence pattern of homogeneously distributed fluorophores in a confocal plane. (**B**) The laser beam (blue cones) is focused in the center of the nucleus during spot bleaching. A bleach time of 4 s (at 3% laser power) was used to allow mobile molecules to diffuse through the laser cone area. Small green spheres represent fluorescent molecules and the green disk represents the confocal plane. (**C**) Theoretical postbleach fluorescence patterns showing 100%, 0%, and 33% immobile molecules. (**D**) Ratio of mean fluorescence intensity (MFI) of pre- and postbleach images [of the theoretical cases shown in (C)] plotted as a function of distance d to the laser spot. Fluorescence ratio is calculated as $(MFI_{d,post} - background)/(MFI_{d,pre} - background)$. The mean immobilized protein fraction p ($0 < p < 1$) of a sample of cells is obtained by least-square fitting of the mean fluorescence ratio profile $FRP_{sample}(d)$ to the weighted sum $FRP_{ws}(d)$ of the fluorescence ratio profiles of nuclei containing immobile molecules only and nuclei containing mobile molecules only: $FRP_{ws}(d) = p * FRP_{100\%immobile}(d) + (1 - p) * FRP_{0\%immobile}(d)$. [(E) to (F)] Procedure for measurement of the average time that molecules stay immobile. (**E**) The fate of the molecules that are immobile at the time of bleaching ($t = 0$) is monitored by recording postbleach images at increasing time intervals after bleaching (fluorescence redistribution time). Molecules that are released during this time interval will diffuse through the nucleus and no longer contribute to the measured immobile fraction. Molecules that become immobilized during the time interval also do not contribute to the measured immobile fraction. (**F**) Theoretical curves of the decay of the measured immobile fraction after bleaching determined by computer simulation of bleaching and diffusion in an ellipsoid volume. The solid line represents the theoretical decay of the measured immobile fraction when molecules are transiently immobile. The intersection with the time axis determines the average binding time—3 min in this example. The dotted lines represent the decay of the measured immobile fraction when a fraction is not transiently immobile, but slowly diffuses through the nucleus.

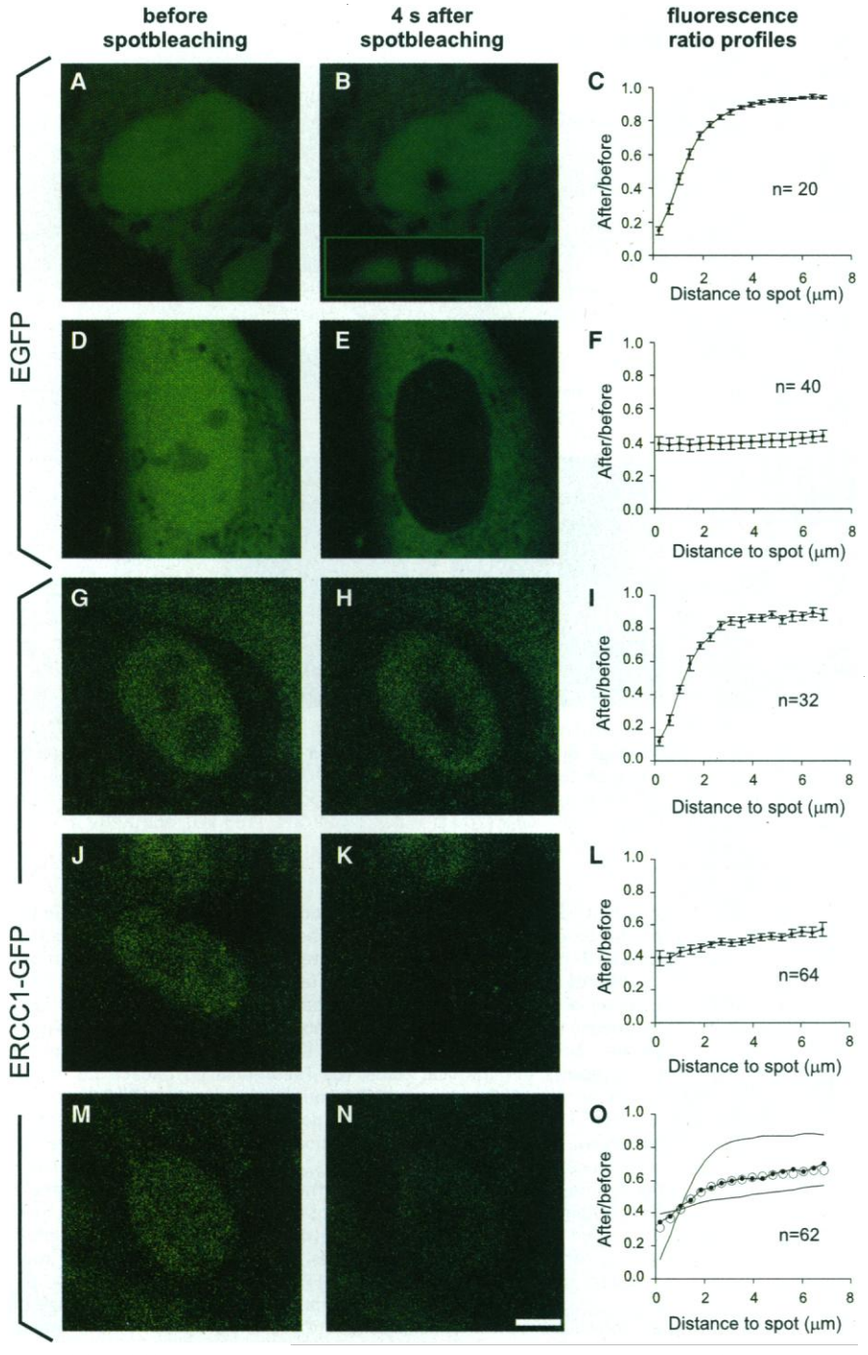

Fig. 3. [(A) to (F)] Application of the FRAP-FIM procedure to human fibroblasts (XPCS2BA-SV40) expressing EGFP. (**A** and **B**) Pre- and postbleach confocal images of EGFP in a fixed fibroblast. Inset in (B) is a confocal z-scan (cross-section) through the nucleus at the site of spot bleaching (compare with the diagram in Fig. 2B). (**C**) FRP of 20 fixed fibroblasts (compare with theoretical curve in Fig. 2D). (**D** and **E**) Pre- and postbleach confocal images of EGFP in a living fibroblast. (**F**) Fluorescence ratio profile of 40 living fibroblasts. [(G) to (O)] Effect of UV irradiation on ERCC1-GFP/XPF mobility. The FRAP-FIM procedure was applied to ERCC1-GFP/XPF-expressing cells that were either (**G** to **I**) fixed in 4% paraformaldehyde, (**J** to **L**) left untreated, or (**M** to **O**) were UV-irradiated. (G), (J), and (M) are prebleach images. (H), (K), and (N) are postbleach images of the same cell. Note that the UV-irradiated cell (N) displays a pattern that is intermediate between that of fixed (H) and untreated (K) cells (compare with Fig. 2C). (I), (L), and (O) are FRPs (compare with Fig. 2D). (**O**) The FRP of UV-irradiated (16 J/m^2) cells (filled circles) optimally fits at $P = 0.35 \pm 0.3$ to the weighted sum (open circles, see legend of Fig. 2D) of fixed and untreated FRPs (solid lines), indicating that 35 ± 3% of the ERCC1-GFP/XPF is immobile (the method of calculation corrects for the overall bleaching that is caused by taking the prebleach image). All images had the same magnification; bar in (O), 5 μm. Error bars in the graphs are two times SEM; *n*, number of cells used for the FRPs.

investigate whether UV-induced NER altered the mobility of ERCC1-GFP/XPF, we applied FRAP-FIM to cells exposed to a UV dose of 16 J/m^2 (Fig. 3, M to O). A significant fraction (35 ± 3%) of ERCC1-GFP/XPF became immobilized within 5 min after UV irradiation, whereas the remaining fraction showed a diffusion rate similar to that in untreated nuclei ($D = 12 \pm 5$ μm^2/s). This suggests that the mobile fraction, in the presence of damage, is not incorporated into a holocomplex. UV irradiation did not cause immobilization of EGFP, RAD52-EGFP (*22*), or GFP-tagged androgen receptor (AR-GFP) (*15, 23*), indicating that the ERCC1-GFP/XPF immobilization is not due to nonspecific UV-induced protein fixation (Fig. 4A).

To quantitate the immobilization, we applied FRAP-FIM to cells exposed to UV doses ranging from 1.6 to 16 J/m^2. The immobilized ERCC1-GFP/XPF fraction increased with UV dose, reaching a plateau of 38 ± 2 % at 8 J/m^2 (Fig. 4B), a dose known to saturate NER. Within 4 to 6 hours following UV exposure [the time required in CHO cells for removal of ~3 × 10^5 6-4PPs induced by a dose of 8 J/m^2 (*24*)] the immobilized fraction progressively decreased to background level (Fig. 4C). Because the amount of DNA damage decreases as a consequence of repair activity, these data strongly suggest that immobilization of ERCC1-GFP/XPF depends on the amount of damage present at any time. Consistent with this, the proportion of immobilized ERCC1-GFP/XPF was inversely related to the expression level of the protein (Fig. 4D). The parallels between repair kinetics and ERCC1-GFP immobilization support the idea that immobilization reflects engagement of the complex in NER. The data in Fig. 4D also suggest that ERCC1-GFP/XPF is not rate-limiting for NER, but is present in excess. Thus, the observed ERCC1-GFP/XPF immobilization may reflect the kinetics of one or more other NER factors.

To investigate how long ERCC1-GFP/XPF complexes are involved in repair, we quantitated the immobile fraction, using FRAP-FIM with increasing redistribution times (Fig. 2, E and F). In this assay, molecules that regain mobility as well as molecules that become immobilized in the period after spot bleaching (fluorescence redistribution time) do not contribute to the measured immobile fraction because they redistribute equally over the nucleus. Within ~4 min after spot bleaching, >95% of the immobile fraction appeared to regain mobility (Fig. 4E). The linear decay suggests that ERCC1-GFP/XPF is immobilized for an average of ~4 min (estimated from the intersection with the time axis; Fig. 2, E and F). The inferred binding time of 4 min is consistent with the estimated time of a single NER event (*25*).

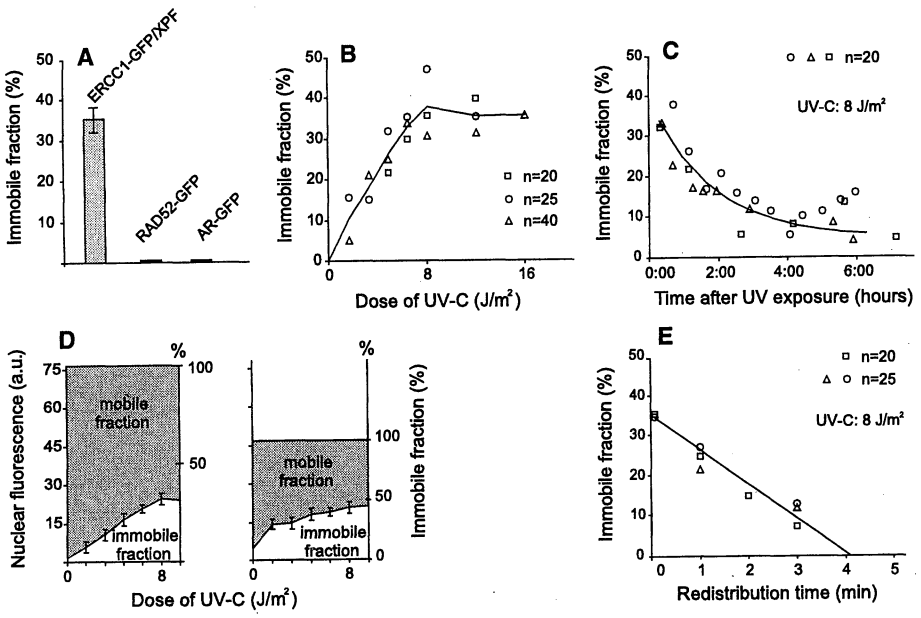

Fig. 4. Response of ERCC1-GFP/XPF to UV irradiation. (**A**) Immobile fraction of ERCC1-GFP/XPF, RAD52-GFP, and AR-GFP after UV irradiation (16 J/m^2). (**B**) Immobile fraction of ERCC1-GFP/XPF plotted against UV dose. The curve represents the average of three independent experiments. Cells with low fluorescence levels were selected for these experiments to exclude from measurements possible overexpressing cells. The number of cells (*n*) used for each experiment is indicated. (**C**) Immobile fraction plotted against time after UV irradiation (8 J/m^2). (**D**) Immobile ERCC1-GFP/XPF (white area) expressed as the percentage of prebleach mean fluorescence (gray+white area) plotted against UV dose. The cells that were used in the experiment represented in (B) were divided into two groups (of equal size) of cells with relatively high (left) and relatively low (right) prebleach fluorescence. Although the immobile fraction is significantly higher in low-fluorescent cells, the actual amount of immobile ERCC1-GFP/XPF is the same in both groups. (**E**) Immobile fraction (8 J/m^2) plotted against fluorescence redistribution time (compare with Fig. 2F). The intersection of the extrapolated curve with the time axis at 4 min indicates that, on average, individual ERCC1-GFP/XPF molecules bind for 4 min.

These data suggest that ERCC1-GFP/XPF is assembled at sites of DNA damage with other NER constituents into immobile holocomplexes during one repair event. After release, ERCC1-GFP/XPF regains full mobility ($D = 12 \pm 5$ μm^2), indicating that it dissociates from the NER/DNA complex.

Our results support a model in which ERCC1-GFP/XPF participates in NER in a distributive fashion. This proposed distributive action contrasts with the processive (DNA-scanning) mechanism that has been reported for NER proteins in prokaryotes (*26*). A distributive mechanism may be more efficient in eukaryotes, because the genome is much larger and contains large stretches of noncoding DNA. However, we have not excluded the possibility that initial detection of DNA damage by the global genome NER initiator XPC/hHR23B (*4*) occurs in a processive fashion. In transcription-coupled repair, damage is probably detected by the elongating RNA polymerase (*2*), which by its nature is processive. Actual repair could take place at the nuclear matrix (*17, 27*).

References and Notes

1. E. C. Friedberg, G. C. Walker, W. Siede, *DNA Repair and Mutagenesis* (American Society for Microbiology, Washington, DC, 1995); R. D. Wood, *Annu. Rev. Biochem.* **65**, 135 (1996); A. Sancar, *ibid.*, p. 43; W. L. de Laat, N. G. J. Jaspers, J. H. J. Hoeijmakers, *Genes Dev.* **13**, 768 (1999).
2. P. C. Hanawalt, B. A. Donahue, K. S. Sweder, *Curr. Biol.* **4**, 518 (1994).
3. D. Bootsma, K. H. Kraemer, J. E. Cleaver, J. H. J. Hoeijmakers, in *The Genetic Basis of Human Cancer*, B. Vogelstein and K. W. Kinzler, Eds. (McGraw-Hill, New York, 1998), pp. 245–274.
4. K. Sugasawa *et al.*, *Mol. Cell* **2**, 223 (1998).
5. J. H. J. Hoeijmakers, J.-M. Egly, W. Vermeulen, *Curr. Opin. Genet. Dev.* **6**, 26 (1996); K. Tanaka *et al.*, *Nature* **348**, 73 (1990); D. Coverley *et al.*, *ibid.* **349**, 538 (1991).
6. W. L. de Laat *et al.*, *Genes Dev.* **12**, 2598 (1998).
7. A. O'Donovan, A. A. Davies, J. G. Moggs, S. C. West, R. D. Wood, *Nature* **371**, 432 (1994).
8. A. M. Sijbers *et al.*, *Cell* **86**, 811 (1996); W. L. de Laat, E. Appeldoorn, N. G. J. Jaspers, J. H. J. Hoeijmakers, *J. Biol. Chem.* **273**, 7835 (1998).
9. A. Aboussekhra *et al.*, *Cell* **80**, 859 (1995); D. Mu, *et al.*, *J. Biol. Chem.* **270**, 2415 (1995).
10. J. Q. Svejstrup *et al.*, *Cell* **80**, 21 (1995).
11. S. N. Guzder, P. Sung, L. Prakash, S. Prakash, *J. Biol. Chem.* **271**, 8903 (1996); *ibid.* **273**, 6292 (1998).
12. D. C. Prasher, V. K. Eckenrode, W. W. Ward, F. G. Prendergast, M. J. Cormier, *Gene* **111**, 229 (1992); M. Chalfie, Y. Tu, G. Euskirchen, W. W. Ward, D. C. Prasher, *Science* **263**, 802 (1994).
13. Humanized GFP-S65T cDNA (Clontech, Palo Alto, CA) was cloned in-frame and downstream of the ERCC1 open reading frame. The resultant cDNA was transfected, using lipofectin (Life Technologies), into ERCC1-deficient (UV-hypersensitive) CHO cells (43-3B). Stable transfectants were selected by growing cells in 800 μg/ml Geneticin (Life Technologies) and by exposing them to UV (4 J/m^2) three times with 1-day intervals. SV40-transformed human fibroblasts were transfected with pEGFP-N1 (Clontech), selected with 300 μg/ml Geneticin, and enriched by fluorescence activated cell sorting. All cell strains were cultured in RPMI medium plus Hepes (Life Technologies) supplemented with 10% fetal bovine serum and maintained in a humidified incubator at 37°C and 5% CO_2.
14. A. J. van Vuuren *et al.*, *EMBO J.* **12**, 3693 (1993); M. Biggerstaff, D. E. Szymkowski, R. D Wood, *ibid.*, p. 3685; C.-H. Park, T. Bessho, T. Matsunaga, A. Sancar, *J. Biol. Chem.* **270**, 22657 (1995); A. M. Sijbers *et al.*, *Nucleic Acids Res.* **24**, 3370 (1996); T. Yagi, R. D. Wood, H. Takebe, *Mutagenesis* **12**, 41 (1997).
15. A. B. Houtsmuller, S. Rademakers, W. Vermeulen, data not shown.
16. S. J. McCready and P. R. Cook, *J. Cell Sci.* **70**, 189 (1984); J. Harless and R. R. Hewitt, *Mutat. Res.* **183**, 177 (1987); L. H. F. Mullenders, A. C. van Kesteren van Leeuwen, A. A. van Zeeland, A. T. Natarajan, *Nucleic Acids Res.* **16**, 10607 (1988); M. S. Park, *Proc. Natl. Acad. Sci. U.S.A.* **93**, 8368 (1996); A. Nakagawa *et al.*, *J. Invest. Dermatol.* **110**, 143 (1998).
17. D. A. Jackson, A. S. Balajee, L. H. F. Mullenders, P. R. Cook, *J. Cell Sci.* **107**, 1745 (1994).
18. D. Axelrod, D. E. Koppel, J. Schlessinger, E. Elson, W. W. Webb, *Biophys. J.* **16**, 1055 (1976); D. E. Wolf, *Methods Cell Biol.* **30**, 271 (1989); N. B. Cole *et al.*, *Science* **273**, 797 (1996).
19. We measured operational diffusion constants as described [J. Ellenberg *et al.*, *J. Cell Biol.* **138**, 1193 (1997); C. L. Wey, M. A. Edidin, R. A. Cone, *Biophys. J.* **33**, 225 (1981)]. In this method, the data were fitted to a one-dimensional diffusion model. The operational diffusion coefficient of EGFP was in the same range as previously reported values, measured with conventional spot-FRAP (*18*) [R. Swaminathan, C. P. Hoang, A. S. Verkman, *Biophys. J.* **72**, 1900 (1997)].
20. For a comparison between MW and *D*, see O. Seksek, J. Biwersi, A. S. Verkman, *J. Cell Biol.* **138**, 131 (1997).
21. XPA and XPB were tagged with EGFP, respectively, at the NH_2- and COOH-termini (S. Rademakers, D. Hoogstraten, W. Vermeulen, unpublished data) and stably expressed in SV40-transformed XP-A and XP-B cells.
22. RAD52 is involved in homologous recombination repair of x ray–induced DNA damage [T. Rijkers *et al.*, *Mol. Cell. Biol.* **18**, 6423 (1998)].
23. The androgen receptor is involved in steroid hormone–dependent transcription regulation.
24. Global genome repair in rodent cells removes predominantly 6-4PPs [D. L. Mitchel, C. A. Haipek, J. M Clarkson, *Mutat. Res.* **143**, 109 (1985); D. L. Mitchell and R. S. Nairn, *Photochem. Photobiol.* **49**, 805 (1989)].
25. Given that a nucleus contains ~30,000 ERCC1-GFP/XPF complexes (J. H. J. Hoeijmakers, unpublished results), of which one-sixth (averaged over the whole repair period; Fig. 4C) is involved in NER, we estimate that damage is repaired at a rate of 1250 lesions per minute ($\frac{1}{6} \times 30{,}000/4$ min). Thus, repair of 300,000 6-4PP lesions (*16*) induced by UV light (8 J/m^2) would require ~4 hours (Fig. 4C).
26. E. Y. Oh and L. Grossman, *J. Biol. Chem.* **264**, 1336 (1989).
27. D. R. Koehler and P. C. Hanawalt, *Nucleic Acids Res.* **24**, 2877 (1996).
28. Immunoblot analysis of total cell extracts (10 μg) and immunoprecipitation of cell lysates were performed as described (*8*). A standard colony-survival procedure for assessment of UV sensitivity (*8*) was applied to CHO-9 (parental repair-competent), 43-3B (ERCC1/repair-deficient), and 43-3B (ERCC1-GFP transfected) cells. At 5 days after UV irradiation (Philips TUV-lamp), the cell survival rate [(number of surviving treated colonies)/(number of surviving untreated colonies)] was plotted against UV dose.

29. We thank P. Berkhout for statistical advice; G. van Cappellen for technical advice; J. Essers and P. Doesburg for cell lines expressing, respectively, RAD52-GFP and AR-GFP; R. van Geloof for software; and R. van Driel, L. H. F. Mullenders, A. A. van Zeeland, and J. Trapman for helpful suggestions. Supported by the Dutch Cancer Society (KWF), the Dutch Scientific Organization (NWO) and by the Louis Jeantet Foundation.

12 January 1999; accepted 26 March 1999